Single-MOSFET DC Thermal Sensor for RF-Amplifier Central Frequency Extraction

Authors: Ferran Reverter[a], Xavier Perpiñà[b], Enrique Barajas[a], Javier León[b], Miquel Vellvehi[b], Xavier Jordà[b], Josep Altet[a]

Affiliation: [a] Department of Electronic Engineering
Universitat Politècnica de Catalunya (UPC) - BarcelonaTech
08034 Barcelona, Spain
[b] Institut de Microelectrònica de Barcelona, IMB-CNM (CSIC)
Campus UAB, Carrer dels Til·lers,
08193 Cerdanyola, Spain

Corresponding author: Ferran Reverter, ferran.reverter@upc.edu
Phone: +34 934137076
Telefax: +34 934137007

View metadata, citation and similar papers at core.ac.uk
brought to you by CORE
provided by UPCommons. Portal del coneixement obert de la UPC

Abstract— A DC thermal sensor based on a single metal-oxide-semiconductor field-effect transistor (MOSFET) is proposed to extract high-frequency electrical features of embedded circuits. The MOSFET sensor is monolithically integrated with the circuit under test (CUT) and then monitors by thermal means the DC power dissipated by the CUT, which carries high-frequency electrical information. After explaining the theory behind this testing approach, the paper demonstrates the feasibility of the proposed MOSFET sensor through simulations and experiments. These are carried out using a radio-frequency (RF) power amplifier as a CUT and thermally extracting its central frequency (440 MHz). The MOSFET sensor results are assessed using an infrared camera as a reference. The main advantage of the proposed sensing method is that the impact on the integrated circuit (IC) layout area is minimum, which is crucial when testing RF-ICs. Moreover, in comparison with previous works, the cost and complexity of the required instrumentation is lower.

Keywords: IC testing; MOSFET; RF testing; temperature sensor; thermal coupling; thermal testing.

1. INTRODUCTION

On-chip thermal sensors are nowadays widely employed [1], and not only in industrial and environmental temperature monitoring applications, but also to compensate for the thermal dependence of other sensors (e.g. piezoresistive sensors), to indirectly measure other parameters (e.g. infrared radiation and humidity), and to monitor the chip thermal profile, which is the application of interest here. Extensive research has been carried out in the development of low-power, small-area on-chip thermal sensors for the thermal management of digital integrated circuits (IC) [2-6]. The aim of these designs is the early detection of hot-spots so as to ensure the reliability and the performance of other embedded circuits. On-chip thermal sensors have also been proposed to test/characterize analog radio-frequency (RF) ICs. The thermal sensor is placed near the RF circuit under test (CUT) and then it measures on-chip thermal variations caused by the power dissipated by the CUT, with the purpose of extracting electrical information. Figures of merit (FOM) such as the central frequency [7-8], the 1-dB compression point (CP) [9], and the DC power drawn [10] have been thermally extracted.

The test/characterization of RF-ICs through on-chip thermal sensors has three main advantages. First, none of the nodes of the RF-CUT is electrically loaded by the thermal sensor and, hence, there is no performance degradation of the RF-CUT. Consequently, a simultaneous co-design of the CUT and the sensor is not required, as it happens in conventional testing strategies based on electrical sensors [11,12]. Second, thanks to the frequency down conversion generated by Joule effect, the sensor output signal shows either a DC level change in a single-tone (homodyne) excitation [8] or a low-frequency (e.g. 1 kHz) sinusoidal signal in a two-tone (heterodyne) excitation [7], regardless of the operating frequency of the RF-CUT. Therefore, the testing setup does not need expensive RF instrumentation at the output. And third, the measurement method not only facilitates a

pass/fail screening in a low-cost high-volume manufacturing test environment, but also enables the on-line monitoring of features during normal operation of the RF-IC. In that sense, on-line self-healing techniques based on thermal sensors have been proposed. For example, in [13], the output signal of the thermal sensor was employed to adjust a tunable load-matching network.

As for the on-chip thermal sensor, the simplest sensing device that can be employed is a diode [10] or a diode-connected transistor, with either a bipolar junction transistor (BJT) [14,15] or a metal-oxide-semiconductor field-effect transistor (MOSFET) [16,17]. BJT-based thermal sensors, which can be fabricated in CMOS technology using parasitic (lateral or substrate) BJTs, have a higher accuracy, but this is not a key element here since the magnitude of interest is the change of temperature caused by the CUT and not its absolute value. MOSFET-based thermal sensors, however, are fully compatible with CMOS technology, have a higher thermal sensitivity especially in strong inversion, and require a smaller layout area [16,17]. This last point is crucial because a small sensing device can be easily fit in empty areas around the CUT with minimum impact on the IC design. Moreover, if the area overhead is minimum, then different thermal sensors can be employed to individually test/characterize each of the blocks of a RF system-on-chip. Thermal measurements can also be carried out using off-chip optical instrumentation, such as an infrared-radiation (IR) camera [18,19], but this is less attractive in terms of cost, integration and on-line monitoring.

This paper aims to prove that a thermal sensor based on a single diode-connected MOSFET measuring DC thermal changes can be employed to extract electrical high-frequency FOM, such as the central frequency of a RF power amplifier (PA). The MOSFET sensor is the same proposed in [9], but the measurement method proposed herein is simpler and requires lower cost off-chip instrumentation. Whereas in [9] the MOSFET sensor measured AC thermal signals resulting from the heterodyne excitation, here it measures DC thermal changes

resulting from the homodyne excitation. Whereas in [9] the sensor output signal was measured by a lock-in amplifier synchronized with the RF signal generator, here it is measured by a low-cost digital multimeter. The extraction of the central frequency of a RF circuit by measuring DC thermal changes has been proposed elsewhere [8, 20], but using more complex sensor topologies not devoid of limitations. These were based on a differential configuration of two BJT sensing devices set to be the differential pair of the input stage of an operational transconductance amplifier. Its main limitations were: (i) a large area around the CUT was required since the sensing device was a parasitic BJT [17], and (ii) a preliminary calibration was needed so as to adjust the mismatch between the two BJT sensing devices and, hence, avoid the saturation of the amplifier output. These limitations are here solved by using a single MOSFET as a thermal sensor, involving a smaller area, no mismatch problems, and fully compatibility with CMOS technology.

The paper is organized as follows. Section 2 describes the case under study. Section 3 provides electrical and thermal simulation results. Section 4 shows the chip designed and its experimental characterization in both electrical and thermal domains. Finally, Section 5 draws the main conclusions.

2. TESTING APPROACH

2.1. Thermal sensor

With the aim of reducing as much as possible the area required and, hence, the impact on the RF-IC layout, we propose to carry out the on-chip thermal measurements through a single MOSFET, which is diode-connected and biased with a DC current source (I_B), as shown in Fig 1(a). Assuming operation in strong inversion, this MOSFET provides an output voltage (v_{out}) that linearly depends on temperature with the following sensitivity [16]

$$S_T = \beta - \frac{\alpha}{2}\frac{1}{T_0}\sqrt{\frac{2I_B}{\mu_0 C_{ox}\frac{W}{L}}}, \qquad (1)$$

where β is the temperature coefficient of the threshold voltage, α is the exponent of the temperature dependence of the mobility, T_0 is a reference temperature, μ_0 is the carriers mobility at T_0, C_{ox} is the gate oxide capacitance per unit area, and W and L are the width and length of the MOSFET channel, respectively. According to (1) and taking into account that $\alpha < 0$, a high (positive) value of S_T can be obtained using a high value of I_B and/or a low value of W/L.

The following three remarks should also be considered for the MOSFET thermal sensor shown in Fig. 1(a). First, although the DC operating point can be quite susceptible to process variations, this is not a major concern here since the information will be in the change of the DC level. Second, I_B is assumed to be unaffected by the power dissipated by the CUT, because either its placement inside the chip will be far enough from the dissipating device or it will be provided by an external bench-top DC current source. And third, the output voltage can also change due to variations of the ambient temperature, but these changes are expected to be much slower than those generated by the test itself and, therefore, the thermal effects of the RF-CUT should be clearly distinguishable.

2.2. RF-CUT

The RF-CUT selected to be tested in the thermal domain is the class-A RF-PA shown in Fig. 1(a), which has a band-pass filter response with a central frequency (f_c) located in the ultra-high frequency (UHF) band and a power gain G_P. The RF input signal (RFin) is connected through a matching network (L_1 in series with C_1) to a MOSFET (M_1) in a common-source topology with resistive feedback (through R_1) and inductive source degeneration (through L_3). This stage is then connected to an inductive load (L_2) through a cascode transistor (M_2), whose bias point is determined by a control voltage (V_{CTL}). At the central frequency, the RF output signal (RFout), which is AC-coupled through C_{out}, has a power that is G_P times higher than that of RFin. The value of the components and the dimensions of the transistors are summarized in Table I.

2.3. Thermal coupling

The CUT and the sensor, located at the top of the die, are thermally coupled through the semiconductor substrate. If the power dissipated by the CUT is in DC, thermal effects are inversely proportional to the distance and, hence, it is advisable to place the thermal sensor as close as possible to the power dissipating device. However, a very short distance can cause a significant CUT-sensor capacitive electrical coupling. On the other hand, if the power dissipated is in AC, the thermal coupling shows a low-pass filter (LPF) response so that the thermal effects of high-frequency power components are filtered out. The cut-off frequency of such a LPF response depends, among others, on the CUT-sensor distance, but values lower than 10 kHz are expected [9].

In the case under study, we propose to place the MOSFET thermal sensor close (say, a few microns) to the cascode transistor [M_2 in Fig. 1(a)] of the RF-PA so as to monitor its power dissipated in DC. The current source (I_B), in case it is embedded into the same chip, should be placed far enough from M_2 (say, tens or hundreds of microns) in order to be unaffected by the dissipated power.

2.4. Homodyne excitation

The thermal characterization of the RF-PA shown in Fig. 1(a) is proposed to be carried out by applying a single RF tone, with a frequency f, to the input, which is known as homodyne excitation [8]. As a consequence of this excitation, the voltages and currents at the main mesh of the circuit have a DC component together with an AC component at f; this is assuming that the relation between the RF voltage applied at the gate of M_1 and the resulting drain-source current is linear. Consequently, the voltage drop and the current through M_2 can be expressed, respectively, as

$$v_2(t) = V_{DC} + V_{AC}\sin(2\pi ft) \tag{2a}$$

$$i_2(t) = I_{DC} + I_{AC}\sin(2\pi ft + \varphi) \tag{2b}$$

where V_{DC} (or I_{DC}) is the DC voltage (or current) level related to the DC operating point of M_2, V_{AC} (or I_{AC}) is the amplitude of the voltage (or current) component at f, and φ is the phase shift between the voltage and current components at f.

Using (2), the power dissipated by M_2 can be calculated as

$$\begin{aligned} p_2(t) = v_2(t)\cdot i_2(t) = \underbrace{V_{DC}I_{DC}}_{\text{Term 1}} + \underbrace{\frac{V_{AC}I_{AC}}{2}\cos\varphi}_{\text{Term 2}} \\ +V_{AC}I_{DC}\sin(2\pi ft) + V_{DC}I_{AC}\sin(2\pi ft+\varphi) \\ -\frac{V_{AC}I_{AC}}{2}\cos(4\pi ft+\varphi) \end{aligned} \quad (3)$$

which has spectral components at DC, f and $2f$. The components at f and $2f$ [i.e. the last three terms in (3)] are expected to be filtered out by the LPF response of the thermal coupling and, therefore, the sensor will not detect thermal oscillations at these frequencies; note that the cut-off frequency of such a LPF is ten thousand times smaller than the minimum value of f under test (i.e. 100 MHz). On the other hand, the power dissipated at DC does generate DC thermal effects in the neighbourhood of M_2. This DC power has two subcomponents: (i) Term 1 that depends on the DC operating point (V_{DC} and I_{DC}), which is expected to be quite independent of f, and (ii) Term 2 that depends on the AC voltage and current amplitudes.

The central frequency of the RF-PA is proposed to be thermally extracted by exploiting the idea that part of the DC power dissipated by M_2 depends on the amplitude of the high-frequency signal [i.e. Term 2 in (3)]. Note that the values of V_{AC}, I_{AC} and φ depend on f and, therefore, the DC temperature (T_s) at the sensor position also depends on f, as qualitatively shown in Fig. 1(b). At the central frequency, where the AC signal is maximally transferred to the output, a minimum value of Term 2 is expected, thus minimizing both the DC dissipated power and T_s. This is proved in the following sections through simulations and experiments.

3. SIMULATIONS

3.1. Electrical simulations

The RF-PA shown in Fig. 1(a) has been electrically simulated in Cadence using V_{DD} = 3.3 V and V_{CTL} = 3.2 V, which are the same values used later in Section 4. A high value of V_{CTL} was employed because it provides a higher value of G_P, but at the expense of a higher current consumption. A high value of V_{CTL} also involves a higher DC power dissipation through both subcomponents [i.e. terms 1 and 2 in (3)], which is beneficial to prove the proposed sensor.

The simulated frequency response of the RF-PA is represented in Fig. 2, for an input power of −10 dBm. The amplifier shows f_c = 550 MHz and G_P = 14.7 dB. Additional simulations were conducted at 550 MHz to determine the 1-dB CP, i.e. the input power that provides an output power that is 1 dBm smaller than that expected in an ideal linear amplifier [21]. Such simulation results are shown in Fig. 3, where we can observe that the relation between the output power and the input power is linear (i.e. slope of one on a log-log scale) at low levels of input power, but it becomes nonlinear at high levels. The 1-dB CP is at −4.5 dBm providing an output power of 9 dBm.

After characterizing the central frequency and the 1-dB CP, we studied through simulations the DC power dissipated by M_2 versus frequency. These simulations were carried out using the Harmonic Balance (HB) method that calculates the magnitude and phase of voltages and currents in steady state at many harmonically-related frequencies, requiring less time and memory than a conventional transient analysis. Fig. 4 shows, for instance, the simulation results for an input power of −10 dBm, where we can observe that the DC power dissipated by M_2 has a minimum at the central frequency (i.e. 550 MHz), as already suggested in Section 2.4. This confirms that the monitoring of the central frequency through thermal measurements is feasible. If the test is done at an input power higher than −10 dBm, the results are very similar to those represented in Fig. 4 but with a higher power change (ΔP). For instance, at −5 dBm input power, which is the limit of the linear region according to Fig. 3, the DC power dissipated by M_2 changes from 100 mW (at 100 MHz) to 90 mW (at 550 MHz).

Simulations in HB also provide the following information: (i) ΔP in Fig. 4 is mainly caused by the DC down-converted power of the RF signal [i.e. Term 2 in (3)]; (ii) the magnitude of DC power components generated by high-frequency harmonics (due to the non-linearity) is at least an order of magnitude lower than Terms 1 and 2; and (iii) the power dissipated by M_1 also has a minimum at the central frequency, but the resulting ΔP is lower than that in M_2.

3.2. Thermal simulations

The thermal effects of having a decrease of the DC dissipated power have been simulated in a 3D structure using the heat-transfer module in COMSOL Multiphysics. It was assumed a silicon substrate with a thickness of 725 μm and without a package, which agrees with that tested later in the experimentation. The boundary conditions considered were [9]: (a) isothermal (20ºC) at the bottom surface, which takes into account that this will be in contact with a high-conductivity large-area metal; and (b) adiabatic at the lateral and top surfaces, which considers that the heat will be mainly transferred by conduction through the silicon substrate towards the bottom [22].

The cascode transistor M_2 in Fig. 1(a) was emulated by three heaters of 19×19 μm^2, as shown in Fig. 5, dissipating each a third of the DC power found before in Section 3.1. The thermal sensor was replaced by a testing point placed in the middle of the empty area between the two first heaters. This geometry, in terms of placement and overall dissipating area, is quite similar to that of the chip fabricated and tested later in Section 4.

Decreasing the DC dissipated power from 100 mW to 90 mW, which corresponds to a −5 dBm input power according to Section 3.1, generates the thermal maps (at the heater depth) shown in Fig. 5. At the sensor position, a $\Delta P = 10$ mW causes a temperature decrease of around 1 ºC (from 27 ºC to 26 ºC). Therefore, if the thermal sensor is able to detect such a DC thermal change, the central frequency of the RF-PA will be thermally monitored. Furthermore, the thermal effects of the DC dissipated power are almost negligible at a distance higher than 45 μm from the center of the heaters. In other words: the temperature at

those distances is almost equal to the reference temperature at the bottom surface (i.e. 20 ºC). Therefore, in a reciprocal way, if the other devices of the RF-PA (e.g. M_1) are appropriately separated from M_2, the measurement of the thermal sensor should be almost independent of the power dissipated by these other devices.

4. EXPERIMENTAL RESULTS AND DISCUSSION

4.1. Chip designed

A chip including the RF-PA and the MOSFET thermal sensor shown in Fig. 1(a) was implemented in 0.35 µm CMOS technology of AMS (AustriaMicroSystems). A microphotograph of the chip layout is shown in Fig. 6. The chip die was then directly soldered, without any package, on a RF board with a large-area metal in contact with the bottom of the chip so as to improve the heat dissipation.

The cascode transistor [M_2 in Fig. 1(a)] was implemented by three transistors ($M_{2,a}$, $M_{2,b}$ and $M_{2,c}$ in Fig. 6) connected in parallel. The MOSFET sensor was placed between $M_{2,a}$ and $M_{2,b}$, as shown in Fig. 6, thus having a geometry similar to that simulated in Section 3.2. The MOSFET sensor had W/L = 1.5/24 and I_B = 20 µA. These values were selected so as to have a high value of S_T (to be precise, 6.3 mV/K in strong inversion [16]), thus facilitating the thermal monitoring. Lower values of W/L and/or higher values of I_B were discarded since they would involve a DC operating point too close (say, higher than 3 V) to the supply voltage of the chip (3.3 V). The layout area occupied by this MOSFET sensor was a thousand times smaller than that of the RF-PA excluding the PAD area, and almost ten times smaller than that required by the substrate BJT included in the design kit.

In terms of power consumption, a sensor bias current of 20 µA is not considered critical here since the RF-PA had a DC current consumption of around 30 mA, which is more than a thousand times higher. If it was critical for another CUT, the dimensions and even the operating mode of the MOSFET sensor should be reconsidered. A low-power low-area

thermal sensor could be obtained using a MOSFET in weak inversion [17]. In such an operating mode, the bias current is in the range of nanoampere, the thermal sensitivity is around −1.6 mV/K that is similar to that provided by a BJT, and the layout area is similar to that occupied in strong inversion, but with W longer than L.

4.2. Electrical test

The chip was first tested using RF instrumentation, as shown in Fig. 7. An RF signal generator (Agilent E4438C, with an output impedance of 50 Ω) provided the RF input signal, whereas a spectrum analyzer (Rohde&Schwarz FSQ26, with an input impedance of 50 Ω) read the RF output signal. In addition, a DC voltage source (Agilent E3646A) provided V_{DD} = 3.3 V and V_{CTL} = 3.2 V.

Fig. 8 represents the experimental frequency response of the RF-PA showing f_c = 440 MHz and G_P = 12.3 dB, for an input power of −10 dBm. In comparison with the simulation results shown in Fig. 2, the experimental values of f_c and G_P were lower. This is probably due to the effects of the parasitic components of the chip-to-board bonding that were not well modeled in the simulations.

Fig. 9 shows the experimental linearity test of the RF-PA carried out at 440 MHz. As in Fig. 3, the relation between the output power and the input power was linear at low levels of input power, but it became nonlinear at high levels. Here, the 1-dB CP was at −2.5 dBm, which is higher than the value obtained in the simulations. This discrepancy is due to the fact of having a lower power gain. In other words: since the power gain is lower, a higher value of input power can be applied before entering to the nonlinear operation region. Note that if the 1-dB CP is referred to the output, both cases (Figs. 3 and 9) show the same value (i.e. 9 dBm).

4.3. Thermal test

Once the actual values of the central frequency and the 1-dB CP were known, the RF-PA was tested in the thermal domain. Instead of measuring the output signal with the spectrum analyzer, we employed the MOSFET thermal sensor to detect the DC thermal change (ΔT)

generated by M_2 at different testing frequencies. The MOSFET sensor was biased by an off-chip DC current source and its output voltage change (ΔV_{out}) was measured by a low-cost digital multimeter (Agilent 34401A) in DC voltage mode, as shown in Fig. 7. In order to validate the on-chip sensor measurements, the setup also had an IR-camera (FLIR SC5500) measuring the temperature changes at the top surface of the chip. Measurements with the MOSFET sensor were conducted at room temperature, whereas those with the IR-camera at 60 ºC (obtained with a thermo-regulated Peltier system) so as to improve its sensitivity and signal-to-noise ratio. IR-measurements were also emissivity corrected at the area between $M_{2,a}$ and $M_{2,b}$ using reference images [23].

The experimental frequency sweep was carried out at −3 dBm input power, which is slightly smaller than the 1-dB CP found in Fig. 9. In such conditions, the RF-PA operated within the linear range and provided a high output power, thus facilitating the thermal detection. Moreover, a −3 dBm input power in Fig. 9 almost yields the same output power that a −5 dBm input power in Fig. 3. Consequently, the experimental DC thermal change was expected to be comparable to that discussed in Section 3.2.

Fig. 10 shows the experimental results of the DC thermal change versus frequency, which qualitatively agree with the simulation results shown in Fig. 4. A negative peak of ΔT was sensed by the MOSFET at 440 MHz, which confirms the idea that the central frequency can be thermally monitored. The DC thermal change detected by the MOSFET sensor at f_c was equal to 2 ºC, which is twice the value estimated in the thermal simulations reported in Section 3.2. Measurements with the IR-camera at the sensor position, also shown in Fig. 10, were qualitatively very similar to those with the MOSFET sensor, but the values of ΔT were smaller. This is probably due to the fact that the top-surface temperature detected by the IR-camera was lower than the substrate temperature measured by the on-chip MOSFET sensor. The decrease of temperature affecting M_2 at f_c is also shown in Fig. 11 through the thermal map monitored by the IR-camera, which is represented as a difference with respect to that

obtained at 100 MHz. Note that at the sensor position, the DC thermal level at f_c is clearly lower than that at 100 MHz, which is illustrated in blue colour in Fig. 11.

6. CONCLUSIONS

This work has gone a step further in the field of IC testing by using a single-MOSFET thermal sensor to extract the central frequency of a RF-PA. The proposed thermal sensor, which relies on a single diode-connected MOSFET, requires a very low area and, hence, it has a very low impact on the IC layout, which is of crucial importance when designing RF-ICs. Moreover, since the information of interest is not in the absolute value of temperature but in the change of temperature, the thermal sensor does not require any calibration. Although the thermal sensor has been applied along the paper to test a RF-PA operating in the UHF band, the same testing approach can be applied to circuits operating at higher frequencies, such as in the millimeter wave band, because the measurement method does not depend on the operating frequency of the circuit.

ACKNOWLEDGEMENTS

This work was supported in part by the Spanish Ministries of Science and Innovation, and Economy and Competitiveness (under the research programs: TEC2013-45638-C3-2-R, Trench-SiC TEC2011-22607, SMARTCELLS TEC2014-51903-R, and Ramón y Cajal RYC-2010-07434), as well as by the regional government of the Generalitat de Catalunya (SGR Grant references 2014 SGR 1596).

REFERENCES

[1] M. Mansoor, I. Haneef, S. Akhtar, A. De Luca, F. Udrea, Silicon diode temperature sensors—A review of applications, Sens. Actuators A 232 (2015) 63-74.

[2] Y.J. An, K. Ryu, D.H. Jung, S.H. Woo, S.O. Jung, An energy efficient time-domain temperature sensor for low-power on-chip thermal management, IEEE Sensors J. 14 (1) (2014) 104–110.

[3] T. Yang, S. Kim, P.R. Kinget, M. Seok, Compact and supply-voltage-scalable temperature sensors for dense on-chip thermal monitoring, IEEE J. Solid-State Circuits 50 (11) (2015) 2773-2785.

[4] S.S. Chouhan, K. Halonen, A low power temperature to frequency converter for the on-chip temperature measurement, IEEE Sensors J. 15 (8) (2015) 4234-4240.

[5] Y.L. Lo, Y.T. Chiu, A high-accuracy, high-resolution, and low-cost all-digital temperature sensor using a voltage compensation ring oscillator, IEEE Sensors J. 16 (1) (2016) 43-52.

[6] K. Ueno, T. Asai, Y. Amemiya, Low-power temperature-to-frequency converter consisting of subthreshold CMOS circuits for integrated smart temperature sensors, Sens. Actuators A 165 (2011) 132-137.

[7] J. Altet. D. Mateo, D. Gómez, J.L. González, B. Martineau, A. Siligaris, X. Aragones, Temperature sensors to measure the central frequency and 3 dB bandwidth in mmW power amplifiers, IEEE Microw. Wireless Compon. Lett. 24 (4) (2014) 272–274.

[8] X. Aragones, D. Mateo, J.L. González, E. Vidal, D. Gómez, B. Martineau, J. Altet, DC temperature measurements to characterize the central frequency and 3 dB bandwidth in mmW power amplifiers, IEEE Microw. Wireless Compon. Lett. 25 (11) (2015) 745-747.

[9] F. Reverter, X. Perpiñà, E. Barajas, J. León, M. Vellvehi, X. Jordà, J. Altet, MOSFET dynamic thermal sensor for IC testing applications, Sens. Actuators A 242 (2016) 195-202.

[10] S.M. Bowers, K. Sengupta, K. Dasgupta, B.D. Parker, A. Hajimiri, Integrated self-

healing for mm-wave power amplifiers, IEEE Trans. Microw. Theory Tech. 61 (3) (2013) 1301-1315.

[11] Q. Yin, W. R. Eisenstadt, R.M. Fox, T. Zhang, A translinear RMS detector for embedded test of RF ICs, IEEE Trans. Instrum. Meas. 54 (5) (2005) 1708-1714.

[12] A. Valdes-Garcia, R. Venkatasubramanian, J. Silva-Martinez, E. Sánchez-Sinencio, A broadband CMOS amplitude detector for on-chip RF measurements, IEEE Trans. Instrum. Meas. 57 (7) (2008) 1470–1477.

[13] Z. Zheng, L. Sun, J. Liu, A 60-GHz power amplifier design with on-chip tunable load-matching network and power detect in 90-nm CMOS, IEEJ Trans. Elect. Electron. Eng. 12 (1) (2017) 140-146.

[14] M.A.P. Pertijs, A.L. Aita, K.A.A. Makinwa, J.H. Huijsing, Low-cost calibration techniques for smart temperature sensors, IEEE Sensors J. 10 (6) (2010) 1098-1105.

[15] A.L. Aita, M.A.P. Pertijs, K.A.A. Makinwa, J.H. Huijsing, G.C.M. Meijer, Low-power CMOS smart temperature sensor with a batch-calibrated inaccuracy of ±0.25ºC (±3σ) from -70ºC to 130ºC, IEEE Sensors J. 13 (5) (2013) 1840-1848.

[16] F. Reverter, J. Altet, MOSFET temperature sensors for on-chip thermal testing, Sens. Actuators A 203 (2013) 234-240.

[17] F. Reverter, J. Altet, On-chip thermal testing using MOSFETs in weak inversion, IEEE Trans. Instrum. Meas. 64 (2) (2015) 524–532

[18] J. León, X. Perpiñà, J. Sacristán, M. Vellvehi, A. Baldi, X. Jordà, Functional and consumption analysis of integrated circuits supplied by inductive power transfer by powering modulation and lock-in infrared imaging, IEEE Trans. Ind. Electron. 62 (12) (2015) 7774–7785.

[19] X. Perpiñà, J. León, J. Altet, M. Vellvehi, F. Reverter, E. Barajas, X. Jordà, Thermal phase lag heterodyne infrared imaging for current tracking in radio frequency integrated circuits, Appl. Phys. Lett. 110 (2017) 094101.

[20] E. Aldrete-Vidrio, D. Mateo, J. Altet, M. Amine Salhi, S. Grauby, S. Dilhaire, M. Onabajo, J. Silva-Martinez, Strategies for built-in characterization testing and performance monitoring of analog RF circuits with temperature measurements, Meas. Sci. Technol. 21 (2010) 075104 (10pp).

[21] B. Razavi, RF Microelectronics, 2nd ed., Pearson, Upper Saddle River (NJ), 2012.

[22] X. Jordà, X. Perpiñà, M. Vellvehi, F. Madrid, D. Flores, S. Hidalgo, J. Millán, Low-cost and versatile thermal test chip for power assemblies assessment and thermometric calibration purposes, Appl. Therm. Eng. 31 (2011) 1664-1672.

[23] M. Vellvehi, X. Perpiñà, G. L. Lauro, F. Perillo, X. Jordà, Irradiance-based emissivity correction in infrared thermography for electronic applications, Rev. Sci. Instrum. 82 (11) (2011) 114901.

List of Figure Captions

Figure 1. (a) Schematic circuit of the RF-PA and the MOSFET thermal sensor. (b) Waveforms of interest from the circuit in Fig. 1(a).

Figure 2. Simulation results of the frequency response of the RF-PA shown in Fig. 1(a), for an input power of −10 dBm.

Figure 3. Simulation results of the linearity test of the RF-PA shown in Fig. 1(a), at a frequency of 550 MHz.

Figure 4. Simulation results of the DC power dissipated by M_2 [i.e. the cascode transistor in Fig. 1(a)] versus frequency, for an input power of −10 dBm.

Figure 5. Simulated plan views of the isothermal lines in steady state, for two values of the DC dissipated power: 100 mW and 90 mW.

Figure 6. Microphotograph of the chip layout including the RF-PA under test and the MOSFET thermal sensor.

Figure 7. Block diagram of the experimental setup employed to electrically and thermally test the RF-PA.

Figure 8. Experimental results of the frequency response of the RF-PA shown in Fig. 1(a), for an input power of −10 dBm.

Figure 9. Experimental results of the linearity test of the RF-PA shown in Fig. 1(a), at a frequency of 440 MHz.

Figure 10. Experimental results of the DC thermal change (measured by the MOSFET sensor and the IR camera) versus frequency, for an input power of −3 dBm; ΔT was calculated using as a reference the temperature obtained at 100 MHz.

Figure 11. Thermal map monitored by the IR-camera at 440 MHz represented as a difference with respect to that obtained at 100 MHz.

List of Table Captions

Table I. Value and dimensions of the components employed in the RF-PA shown in Fig. 1(a). [(a)] It is composed of an on-chip inductance (5 nH) plus the bond-wire inductance. [(b)] Parasitic inductance mainly generated by the bond wire and the PCB track. [(c)] Parasitic inductance generated by the bond wire; it is smaller than L_2 since the CUT has several pads (V_{SS} in Fig. 6) connected to ground.

Figure 1

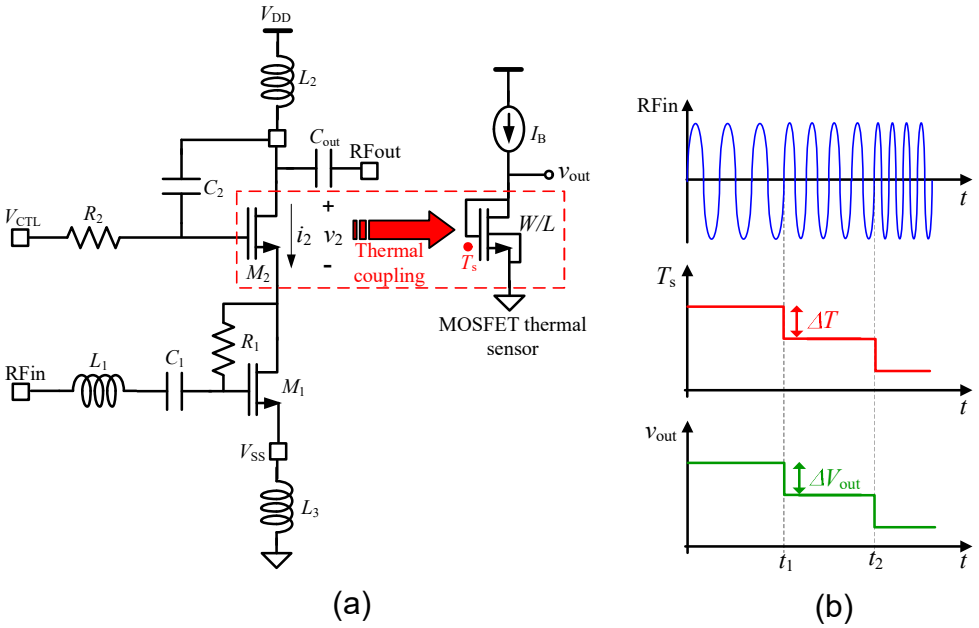
V_{DD}
L_2
C_{out}
RFout
I_B
v_{out}
C_2
V_{CTL}
R_2
i_2
v_2
Thermal coupling
T_s
W/L
M_2
MOSFET thermal sensor
R_1
RFin
L_1
C_1
M_1
V_{SS}
L_3
(a)
RFin
t
T_s
ΔT
t
v_{out}
ΔV_{out}
t_1
t_2
t
(b)

Figure 2

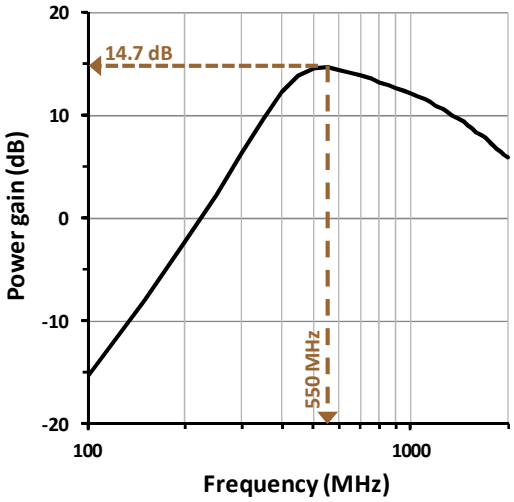
20
10
0
-10
-20
14.7 dB
550 MHz
Power gain (dB)
100
1000
Frequency (MHz)

Figure 3

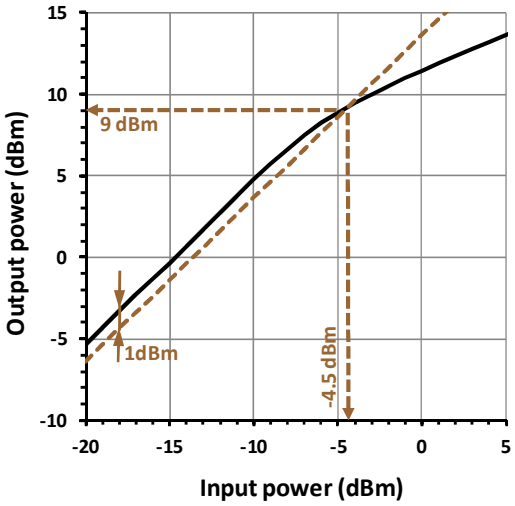
15
10
5
0
-5
-10
-20
-15
-10
-5
0
5
Output power (dBm)
Input power (dBm)
9 dBm
1dBm
-4.5 dBm

Figure 4

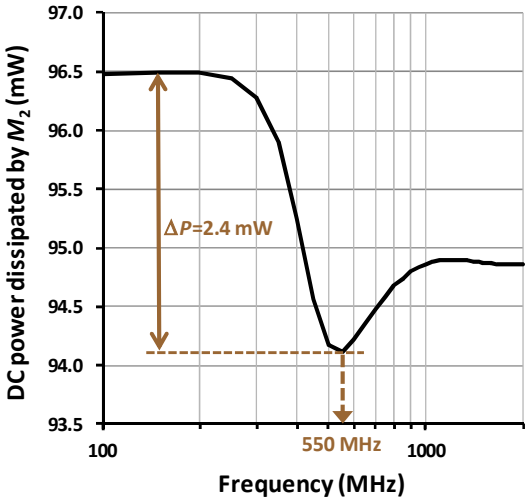
97.0
96.5
96.0
95.5
95.0
94.5
94.0
93.5
DC power dissipated by M_2 (mW)
ΔP=2.4 mW
550 MHz
100
1000
Frequency (MHz)

Figure 5

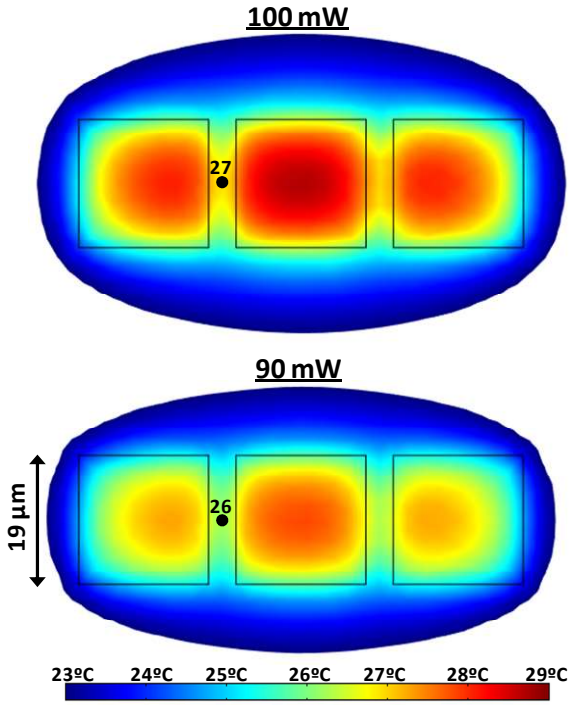

Figure 6

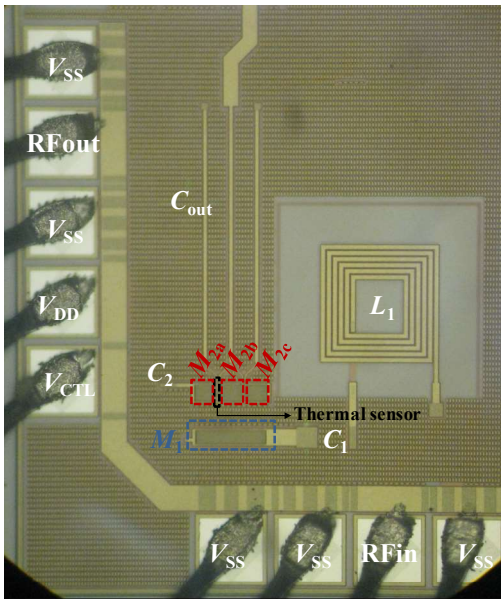
V_{SS}
RFout
V_{SS}
V_{DD}
V_{CTL}
C_{out}
L_1
C_2
M_{2a}
M_{2b}
M_{2c}
Thermal sensor
M_1
C_1
V_{SS}
V_{SS}
RFin
V_{SS}

Figure 7

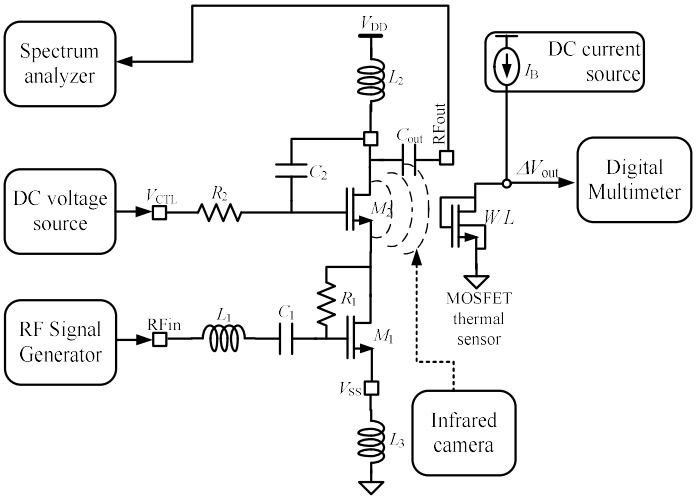
Spectrum analyzer
DC voltage source
RF Signal Generator
DC current source
Digital Multimeter
MOSFET thermal sensor
Infrared camera
V_{DD}
L_2
C_{out}
RFout
C_2
V_{CTL}
R_2
M_2
WL
ΔV_{out}
I_B
R_1
RFin
L_1
C_1
M_1
V_{SS}
L_3

Figure 8

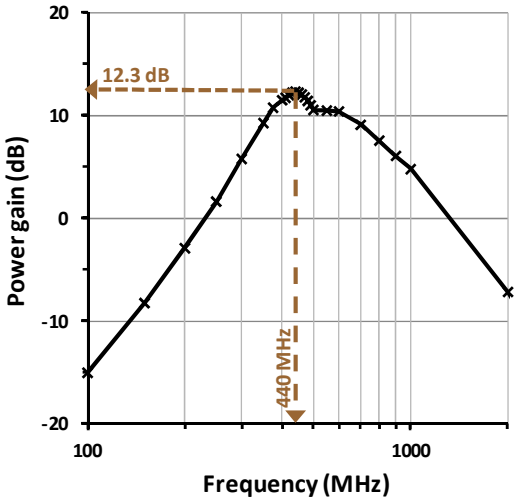
20
10
0
-10
-20
12.3 dB
440 MHz
Power gain (dB)
100
1000
Frequency (MHz)

Figure 9

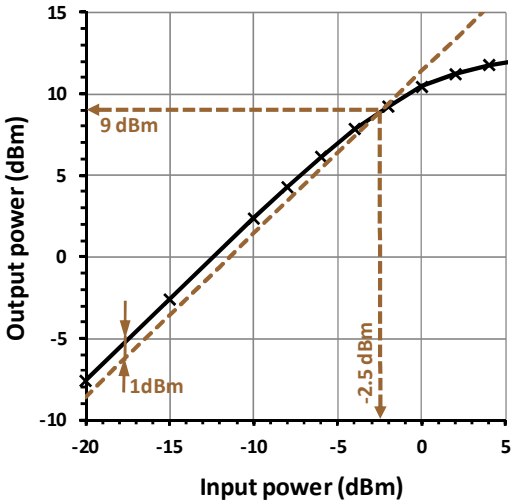
15
10
5
0
-5
-10
-20
-15
-10
-5
0
5
Output power (dBm)
Input power (dBm)
9 dBm
1dBm
-2.5 dBm

Figure 10

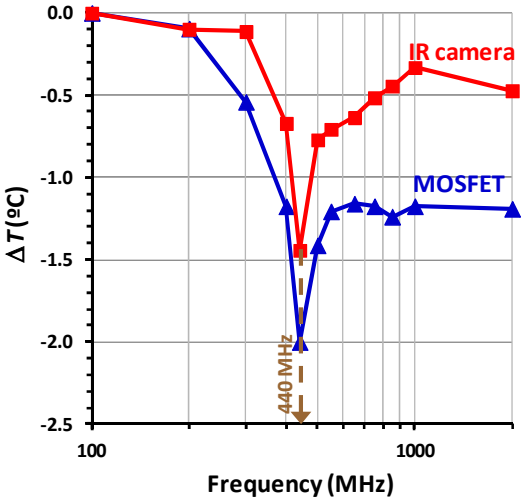
0.0
-0.5
-1.0
-1.5
-2.0
-2.5
ΔT (ºC)
100
1000
Frequency (MHz)
IR camera
MOSFET
440 MHz

Figure 11

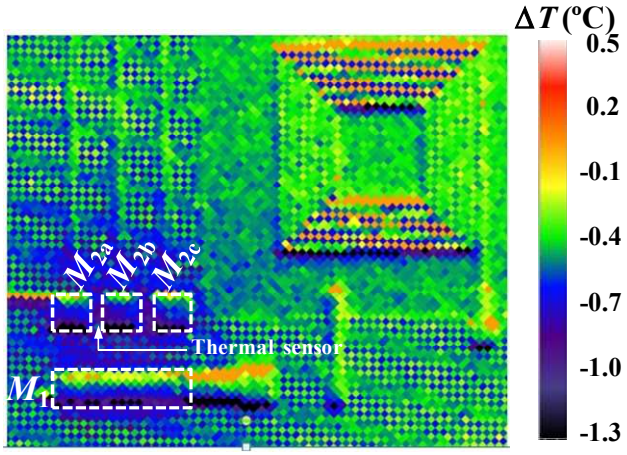

Table I

Component	Value or dimensions
R_1	6428 Ω
R_2	6428 Ω
C_1	5 pF
C_2	1 pF
C_{out}	5 pF
L_1	12.2 nH [(a)]
L_2	19.2 nH [(b)]
L_3	1.4 nH [(c)]
M_1	W = 1159 μm, L = 0.5 μm, 61 fingers
M_2	W = 1173 μm, L = 0.5 μm, 51 fingers